Modeling spatial intercellular communication and multilayer signaling regulations using stMLnet

Jingyu Cheng [1], Lulu Yan [2], Qing Nie [3], Xiaoqiang Sun [2*]

1. School of Medicine, Sun Yat-sen University, Guangzhou 510080, China.
2. School of Mathematics, Sun Yat-sen University, Guangzhou 510275, China.
3. Department of Mathematics and Department of Developmental & Cell Biology, NSF-Simons Center for Multiscale Cell Fate Research, University of California Irvine, Irvine, CA 92697, USA.

* To whom correspondence should be addressed.

Xiaoqiang Sun. E-mail: sunxq6@mail.sysu.edu.cn

Abstract

Multicellular organisms require intercellular and intracellular signaling to coordinately regulate different cell functions. The technological advance of spatial transcriptomics (ST) lets us leverage spatial information to better elucidate cell signaling and functioning. Here, we present stMLnet, a method that infers spatial intercellular communication and multilayer signaling regulations from ST data by quantifying distance-weighted ligand–receptor (LR) signaling activity based on diffusion and mass action models and mapping it to intracellular targets. We demonstrated the applicability of stMLnet on a breast cancer ST dataset and benchmarked its performance using multiple cell line perturbation datasets, synthetic data, and LR-target correlations stratified by cellular distance. We then applied stMLnet to an ST dataset of SARS-CoV-2-infected lung tissue, revealing positive feedback circuits between alveolar epithelial cells, macrophages, and monocytes in a COVID-19 microenvironment. Furthermore, we applied stMLnet to analyze glioma-macrophage interactions for deciphering intercellular and intracellular signaling mechanisms underlying immunotherapy resistance in gliomas. Our proposed method provides an effective tool for predicting LR-target regulations between interacting cells, which can advance the mechanistic and functional understanding of cell–cell communication.

Keywords

Cell–cell communication / Modeling and inference / Multilayer signaling network / Spatial transcriptomics

Introduction

It has become increasingly clear that cell fates and functions are not only determined by the intrinsic genetic makeup of the cell, but they are also influenced by neighboring cells and the spatial environment in multicellular tissue (Boulanger *et al*, 2007; Scadden, 2006). Recent studies have revealed that cell–cell interactions (CCIs) play important roles in cell differentiation, tissue development, immunity, and cancers (Pires-daSilva & Sommer, 2003). Elucidating the mechanisms by which intercellular signaling regulates intracellular gene expression is essential to advance our understanding of the functional and therapeutic roles of CCIs (Armingol *et al*, 2021).

Cells can interact with each other in multiple ways, such as physical cell–cell contact (e.g., cell adhesions) (Boisset *et al*, 2018; Parsons *et al*, 2010) and biochemical cell–cell communication (CCC) mediated by diffusible molecules (e.g., autocrine, paracrine or endocrine via ligand–receptor (LR) interactions) (Armingol *et al*, 2021). CCC plays vital roles in many physiological functions of multicellularity, and its dysregulation often drives the occurrence and development of many diseases (Heasley, 2001). CCC generally involves four sequential events (Krauss, 2014): 1) secretion and diffusion of ligand molecules; 2) reception and specific binding of the ligand by the receptor, leading to receptor activation; 3) induction of one or multiple signaling transduction pathways by the activated receptors, leading to the activation of downstream transcriptional factors (TFs); and 4) regulation of target gene expression by the activated TFs and initiation of cell phenotype switching. Together, the signaling mechanisms involved in functional CCC include both intercellular LR interactions and intracellular signaling transduction and transcriptional regulation, which is referred to as the multilayer signaling network (Almet *et al*, 2021; Cheng *et al*, 2020; Zhang *et al*, 2020). Traditional experimental studies have often focused on a single or a few signaling molecules to study intercellular communications, lacking information across multiple scales of signaling. Systems analysis of signaling regulations in functional CCC is challenging and critical.

Single-cell RNA sequencing (scRNA-seq) provides unprecedented high-throughput data to decipher intercellular communication by analyzing cell-type-specific expression of ligands and receptors (Armingol *et al*, 2021). Recently, several computational methods or tools have been developed to infer CCC from scRNA-seq data (Almet *et al*, 2021; Armingol *et al*, 2021). However, most existing methods or tools (e.g., (Cang & Nie, 2020; Efremova *et al*, 2020; Jin *et al*, 2021; Wang *et al*, 2019b)) only consider intercellular LR signaling pairs without dissecting the response of their downstream pathways (see a comprehensive comparison of related methods in **Table S1**).

Previously we developed a multilayer network approach to infer both intercellular and intracellular signaling networks (Cheng *et al*, 2021; Ni *et al*, 2022; Zhang *et al*, 2020). While several other methods (e.g., (Browaeys *et al*, 2020; Zhang *et al*, 2021)) also consider intracellular responses, the information of cellular distance affecting the transportation and reception of secretory molecules across the spatial environment is missing because of the loss of the positional information of cells in the scRNA-seq data. Recently, the rapid advancement of spatially resolved sequencing technology that measures both gene expression and positional

information of cells (Longo *et al*, 2021) has afforded new opportunities to infer spatial and functional CCC (Walker *et al*, 2022).

In this study, we present stMLnet, a spatial transcriptomics (ST)-based multilayer network method for inferring spatial intercellular communication and LR-target gene regulations. stMLnet mechanistically quantifies cell-distance-dependent LR signaling activity based on a mathematical model of ligand diffusion and the LR reaction, and it quantitatively maps the intercellular LR signals to intracellular gene expressions using explainable tree-based machine learning. Our method can prioritize ligands, receptors, or their pairs that regulate specific target genes. We demonstrated stMLnet on an ST dataset of breast cancer and evaluated its predictive accuracy using cell line perturbation data, simulation data, and differential LR-target correlations in distal and proximal cell pairs. After benchmarking stMLnet with other methods, we applied stMLnet to analyze CCIs underlying the inflammatory response to COVID-19 infection and to decipher intercellular and intracellular signaling mechanisms underlying immunotherapy resistance in gliomas.

Results

Overview of stMLnet

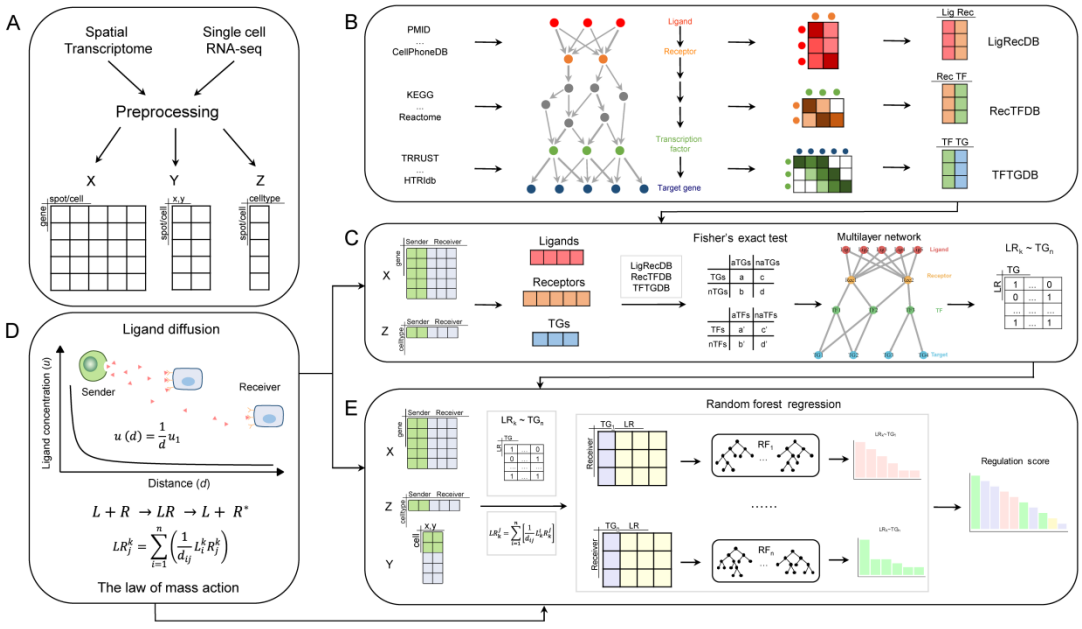

Fig 1. *stMLnet framework*. *(**A**) Inputs of stMLnet. (**B-E**) Workflow of stMLnet. (**B**) Integration of prior network information. stMLnet integrates prior information from multiple data sources of molecular interactions, including LR interaction, signaling pathways, and transcriptional regulations, into prior knowledge databases of stMLnet (i.e., LigRecDB, RecTFDB, and TFTarget DB) by the directed weighted graph and random walk algorithm. (**C**) Statistical inference of multilayer signaling network. Based on the transcriptomic data and the prior information, stMLnet employs the statistical test method to infer the multilayer signaling network and obtain the correspondence between LR pairs and the downstream target genes (TGs) (LR~TG). (**D**) Quantification of LR signaling activity. Based on the ligand diffusion model and the law of mass action, the LR signaling activity is modeled as a distance-dependent function. (**E**) Random*

forest regression links LR activity to target gene expression. Explainable importance score of the k_t-th feature (LR_{k_t}) contributing to the target expression G_t was computed to prioritize the upstream ligands or receptors regulating target genes.

Our proposed method aims to infer, quantify, and visualize both intercellular communications and the intracellular gene regulatory network from ST data with an emphasis on the impact of spatial cellular distance in CCCs (**Fig 1**). First, stMLnet integrates multiple data sources of molecular interactions (including LR interaction, signaling pathways, and transcriptional regulations) (**Text S1**) into in-house knowledge databases (i.e., LigRecDB, RecTFDB, and TFTargetDB) by using the directed weighted graph and random walk algorithm (**Text S2**) (**Fig 1B**). Second, based on the prior network information and the gene expression data, stMLnet uses Fisher's exact test to infer the structure of the multilayer signaling network (**Text S4**) and obtain the paths from LR pairs to the downstream targets (LR~TG) (**Fig 1C**). Third, to quantify LR signaling activity, stMLnet mechanistically models the LR signaling activity as a cell-distance-dependent function based on a ligand diffusion model and the law of mass action (**Fig 1D**). Lastly, to model the nonlinear LR-TG regulation relationships, stMLnet employs an explainable tree-based modeling approach (e.g., random forest regression) to link LR activity to target gene expression, with feature importance ranking to measure the contribution of each upstream ligand and/or receptor to the target gene expression (**Fig 1E**).

The ***input*** of stMLnet includes the gene expression matrix (gene×spot) ($\boldsymbol{X}$), cell location matrix (spot×dim) ($\boldsymbol{Y}$), and cell type matrix (spot×annotation) ($\boldsymbol{Z}$) to indicate the cell type annotation and labels of receiver cells and/or sender cells. The cell location matrix is used to calculate the cell distance matrix ($\boldsymbol{D}$). In addition, stMLnet also allows inputs of a set of genes of interest as target genes for analysis. The ***output*** of stMLnet includes the multilayer signaling network (LR-TF-TG), LR signaling activity, and importance ranking of LR or L/R with respect to their ability to regulate target gene expression. stMLnet also provides various ***visualizations*** of the results, for instance, the circle plot of the CCC network, edge bundling plot of intercellular LR activity, waterfall plot of multilayer signaling network, multilayer network visualization of sub-networks downstream of a specified ligand, and heatmap of functional enrichment for ligands/receptors based on downstream target genes.

Demonstration of stMLnet on an ST dataset of breast cancer

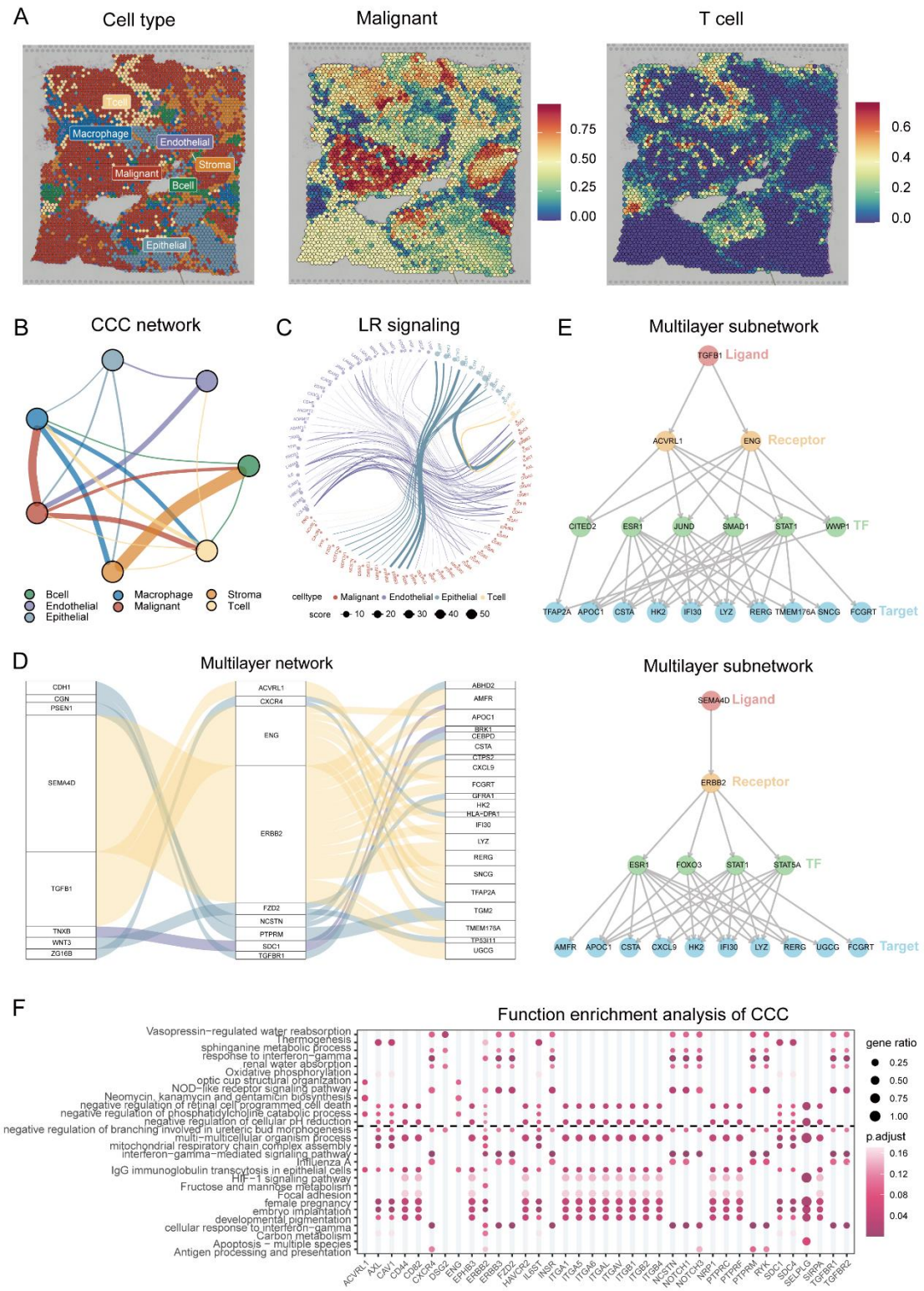

Fig 2. ***Application of stMLnet to an ST dataset of breast cancer***. *(**A**) The cell type annotation for spots in the ST data and the cell type proportion distribution of malignant cells and T cells. (**B**) The CCC network. Different node colors represent different cell types. The edges represent intercellular communications from the sender cells to the receiver cells. The edge color is consistent with that of the sender cells, and the edge width represents the number of LR pairs. (**C**) The edge bundling plot of LR signaling activity (top ranked). The nodes represent ligands or receptors, with different colors for different cell types. The edges*

*represent LR signaling from the sender cells (e.g., T cells, endothelial cell, and epithelial cells) to the receiver cells (e.g., malignant cells here), with the edge color being consistent with that of the sender cell. The node size or edge width indicates the average strength of the LR signaling. (**D**) The waterfall plot of the multilayer signaling network. Regulatory paths from upstream LR pairs (top ranked) to their downstream targets in malignant cells are shown. The path color indicates the cellular source (sender cells) of the ligand signaling, and the path width represents the importance score of each LR with respect to TG regulation. (**E**) The multilayer signaling subnetwork indicates the regulatory paths from a specified ligand/receptor to its downstream TFs and then to target genes. Regulatory networks downstream of TGFB1 (up) or SEMA4D (below) in malignant cells are shown. Top-ranked target genes according to importance scores are prioritized for visualization. (**F**) Heatmap of functional enrichment for CCC. The GO biological process (BP) (up) or KEGG (below) enrichment of the downstream targets for a set of upstream receptors during CCI with T cells as senders and malignant cells as receivers is shown. Top-ranked function terms according to p-values were prioritized for visualization.*

To globally analyze CCCs between different cell types, including malignant cells, T cells, B cells, macrophages, epithelial cells, endothelial cells, and stromal cells, in the tumor microenvironment of breast cancer (**Fig 2A**, **Fig S4**), we applied stMLnet to infer the multilayer signaling networks for all pairs of sender cells and receiver cells. The interaction-changed genes (ICGs) (Dries *et al*, 2021a) in each type of receiver cell were selected as the corresponding target genes of interest. The circle plot of the CCC network (**Fig 2B**) demonstrates abundant interactions between different cell types in the tumor microenvironment.

To decipher microenvironmental regulatory mechanisms of the target genes in the breast cancer cells, we focused on the inferred multilayer network with the malignant cells as the receiver and other cell types as senders. The edge bundling plot of LR interactions (**Fig 2C**) shows LR signaling from various sender cells, including T cells, endothelial cells, and epithelial cells, to the malignant cells. Different LR pairs possessed varied signaling activities, depending on both ligand/receptor expression levels and sender–receiver cell distances. Furthermore, the waterfall plot of the multilayer signaling network (**Fig 2D**) shows regulatory paths from upstream LR pairs (top ranked) to their downstream targets in malignant cells. Based on the computed (partial) importance scores (**Text S5**), we could prioritize upstream LR regulators for given target genes or downstream targets for a specified ligand/receptor. For instance, TGFB1 and SEMA4D, expressed by T cells, deliver intense signals to interact with their receptors (ENG and ERBB2, respectively) and contribute largely to the regulation of a number of target genes.

In addition, the multilayer signaling subnetwork (**Fig 2E**) indicates the signaling paths from a specified ligand to the corresponding receptor(s), and then to downstream TFs and target genes. As shown, TGFB1 regulated the downstream target genes through pathways that activate TFs, including SMAD1, STAT1, and WWP1 in malignant cells, while the pathways downstream of SEMA4D-ERBB2 signaling activated TFs, including ESR1, FOX3, and STAT1/5.

To infer biological functions of the intercellular communication, we performed GO BP and KEGG pathway enrichment for the downstream target genes of each receptor. The heatmap of functional enrichment (**Fig 2F**) shows that a panel of pathways or biological processes related to immunology or metabolism was dysregulated, indicating microenvironment-induced alterations of the functional states of malignant cells.

Testing and benchmarking stMLnet using cell line perturbation data

A

	Lig/Rec	Condition	Cell Line	AUCROC	AUCPR
GSE157680	NRP1	Knockdown	MDA-MB-231	0.9444	0.9167
GSE15893	CXCR4	Mutant	MDA-MB-231	0.7976	0.8049
GSE160990	TGFB1	Treatment	MDA-MB-231	0.7778	0.9223
GSE54329(1)	IL6	Treatment	EFM-19	0.5714	0.3333
GSE54329(2)	IL6	Treatment	HCC1428	0.9655	0.75
GSE54329(3)	IL6	Treatment	MDA-MB-134VI	0.6429	0.3778
GSE54329(4)	IL6	Treatment	MDA-MB-175-VIIdsRed	0.7241	0.5556

B

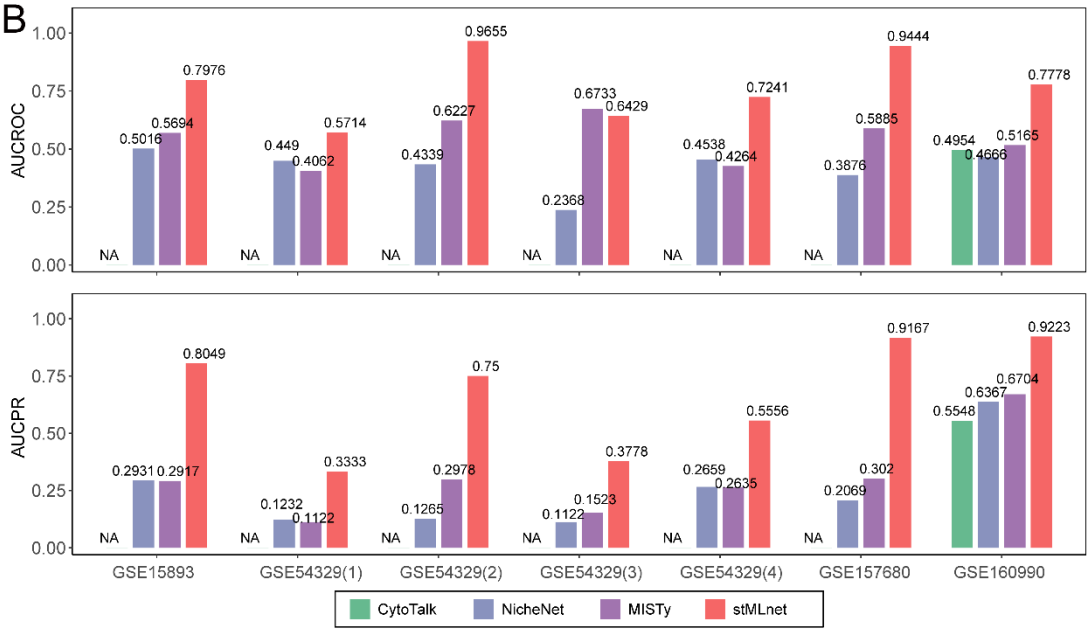

Fig 3. ***Benchmarking stMLnet against other methods using cell line perturbation data****. The predicted L/R-targets regulations were validated by testing whether the targets were differentially expressed in 7 datasets of breast cancer cell lines under corresponding L/R perturbation conditions (e.g., TGFB1 or IL6 stimulation, NRP1 knockout, or CXCR4 mutation). The prediction accuracy of stMLnet was compared to that of CytoTalk, NicheNet, or MISTy, assessed by AUCROC and AUCPR. 'NA' indicates that the corresponding ligands or receptors used for cell line perturbation could not be inferred by CytoTalk.*

To test the accuracy of the LR-target prediction of stMLnet on the breast cancer ST dataset, we collected 7 datasets of breast cancer cell lines with different perturbation conditions (e.g., TGFB1 or IL6 stimulation, NRP1 knockout, or CXCR4 mutation) (**Fig 3A**). If the downstream target genes are differentially expressed, they are considered to be potentially regulated by the corresponding ligand or receptor. As such, it is reasonable to use the differentially expressed genes (DEGs) as the ground truth of downstream targets of a specific ligand or receptor (Browaeys *et al*, 2020; Zhang *et al*, 2021). To this end, we compared the predicted partial importance scores of the corresponding ligand or receptor on the target genes (**Text S5**) with the ground truth (i.e., the differential expression status (true or false) of the target genes in each cell line after perturbation) and evaluated the prediction accuracy using AUCROC and AUCPR. The result (**Fig 3B**) indicates that stMLnet had good predictive accuracy on most datasets (AUCROC was greater than 0.72, and AUCPR was greater than 0.55 on 5 of 7 datasets).

We compared stMLnet with other methods of CCC inference or L/R-target regulation prediction. **Table S1** lists their characteristics, such as model/algorithm, input, intercellular prediction, intracellular prediction, and spatial information utilization. Among them, NicheNet (Browaeys *et al*, 2020), CytoTalk (Zhang *et al*, 2021), and MISTy (Tanevski *et al*, 2021) were selected for quantitative benchmarking, as these three methods could predict L/R-target regulation. The implementation of these methods for benchmarking is described in **Text S7**. We compared their prediction accuracy (AUCROC and AUCPR) with that of stMLnet by using the cell line perturbation data, as described above. The results (**Fig 3B**) show that stMLnet significantly outperformed the other three methods on all 7 datasets.

Analysis of distance-weighted LR signaling activity

In the stMLnet model, the LR signaling activity is dependent on the spatial distance between the sender cell and the receiver cell (Equation (5)). To analyze the distance-weighted LR signaling activity, we substituted the reciprocal distance weight ($\frac{1}{d_{ij}}$) in LR signaling activity with the alternative constant weight (1) or exponential weight ($e^{-\frac{d_{ij}^2}{2l^2}}$), and we compared the performance of stMLnet with the two variants. We compared the prediction accuracies of LR-target regulation based on the above three distance weights using cell line perturbation data (as used in **Fig 3**). Various evaluation metrics, including AUCROC (area under the ROC curve), AUCPR (area under the Precision/Recall curve), PPV (positive predictive value), Accuracy, Error rate, and MCC (Matthews correlation coefficient), were used for assessment. All of the above evaluation metrics were averaged on the 7 cell line datasets, and stMLnet consistently performed better than the other two variants, favoring the reciprocal distance weight for modeling LR signaling activity (**Fig 4A**).

To scrutinize the distance-weighted LR signaling activity, we performed a simulation study based on a mathematical model of ligand diffusion and L-R-TF-Target regulation (see details in the Methods section) to generate 100 sets of synthetic data (**Fig S3**). The simulated spatial expression data were used as input of stMLnet (without using the prior information of the predefined multilayer network) to infer the regulation of TGs' expression by LR pairs. The predicted importance scores for LR-TG regulations were benchmarked with the ground truth of the simulated network topology. The evaluation of the 6 metrics, namely, AUCROC, AUCPR, Accuracy, PPV, Error rate, and MCC, on 100 synthetic datasets (**Fig 4B**) showed that the reciprocal distance weight significantly outperformed the other two variants. These results affirm the rationality and effectiveness of stMLnet in modeling spatial distance-dependent cell communication and gene regulation.

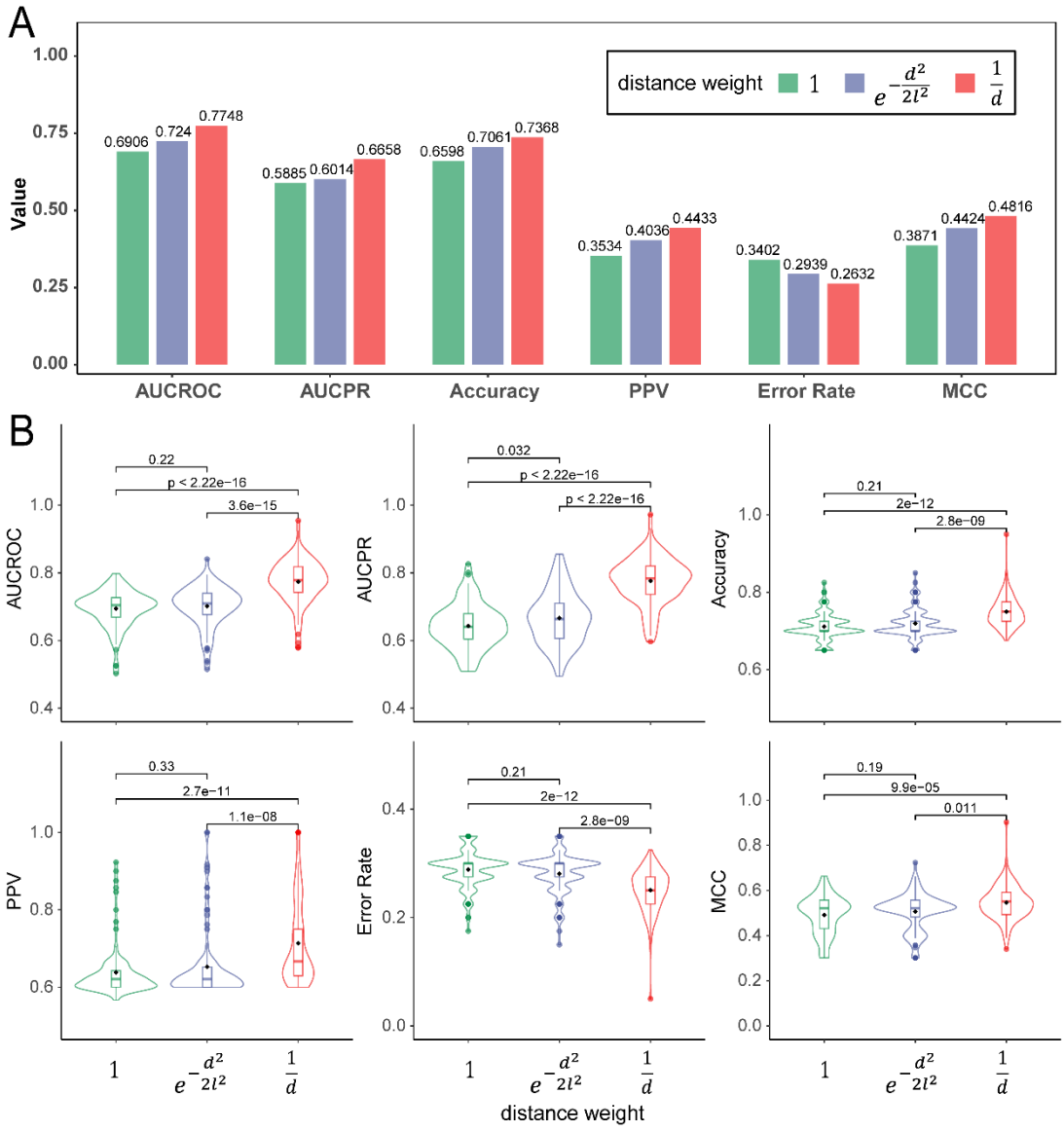

Fig 4. ***Analysis of distance-weighted LR signaling activity***. *The performance of stMLnet in LR-target prediction was compared to that of its variants with modified distance weights of LR activity scoring. The distance weights are the reciprocal function (i.e.,* $\frac{1}{d}$*) in stMLnet and exponential function (i.e.,* $exp\ (-\frac{d^2}{2l^2})$*) or constant function (i.e.,* 1*) in its two variants, respectively. (**A**) Based on cell line perturbation data, the performances of stMLnet and the two variants were evaluated and compared. The evaluation metrics (AUCROC, AUCPR, Accuracy, PPV, Error rate, and MCC) were averaged on 7 cell line datasets. (**B**) Based on 100 synthetic datasets, the performances of stMLnet and the two variants in predicting LR-target regulation were evaluated and compared. The Wilcoxon rank sum test p value was used to assess the statistical significance.*

Evaluating stMLnet based on LR-target correlations

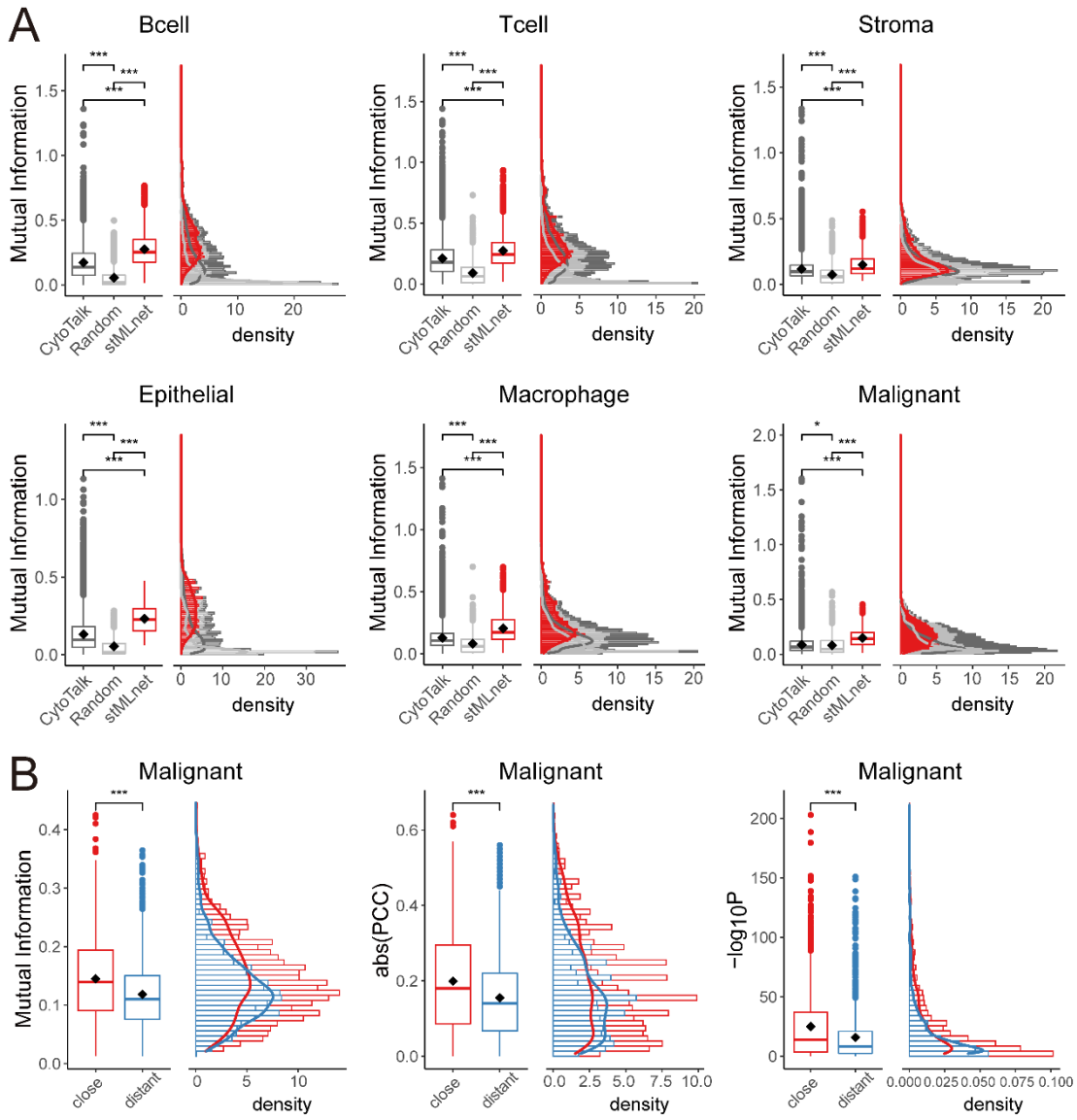

Fig 5. ***Evaluating stMLnet based on LR-target correlations***. *(**A**) Distributions of mutual information between LR signaling activities and target gene expressions (LR_{k_t}~TG_t) in different cell types. The LR-target pairings predicted by stMLnet had larger mutual information values than other methods (e.g., CytoTalk) and random pairing. (**B**) Correlation of LR_{k_t}~TG_t predicted by stMLnet in malignant cells stratified by close or far distance to the sender cells. The close group had higher correlation than the distant group, assessed by the mutual information, the absolute value of PCC, and the –log10(p value of PCC).*

To further evaluate the predictions of stMLnet regarding LR-target regulations, we hypothesized that the more reliable the inferred network, the higher the correlation between LR signaling activity and target gene expression. As such, we computed the mutual information (MI) or the Pearson correlation coefficient (PCC) for each pair of LR_{k_t}~TG_t $(t = 1, 2, \ldots, m;\ k_t = 1, 2, \ldots, n_t)$ in the multilayer networks inferred by stMLnet based on the breast cancer ST dataset.

We then compared values of MI or PCC of $LR_{k_t}{\sim}TG_t$ with that of random pairing or that inferred by other methods. Here, only CytoTalk could be used for comparison, as NicheNet predicts ligand-target regulations but does not involve receptors, and MISTy does not explicitly model LR interactions. The LR-target pairings predicted by stMLnet had larger MI values than CytoTalk and random pairing, across various cell types (**Fig 5A**). In addition, evaluations using PCC or –log10(p value of PCC) (**Fig S5**) consistently showed that stMLnet exhibited higher LR-target correlations than CytoTalk and random pairing.

Closer cells have a larger probability to communicate with each other, so intercellular signaling should have a stronger impact on intracellular gene expression. To further inspect LR-target correlations of stMLnet, we divided sender-receiver pairs, based on cellular pairwise distances, into a close group (cell pairs with a distance less than the 25th percentile of all of the pairwise distances) and distant group (cell pairs with distance greater than the 75th percentile of all of the pairwise distances). We set malignant cells as receivers and examined whether the close group had a higher correlation (MI or PCC) between LR signaling activity and the target gene expression than the distant group. The results (**Fig 5B**) show that both MI values and PCC values as well as –log10(p value of PCC) of the predicted $LR_{k_t}{\sim}TG_t$ were larger in the close group than in the distant group. These results further verify the reliability of stMLnet in LR-target predictions.

stMLnet revealed positive feedback circuits between alveolar epithelial cells, macrophages, and monocytes in a COVID-19 microenvironment

We applied stMLnet to a set of ST data of COVID-19-infected lung tissue (**Fig 6A**) to investigate CCIs underlying the inflammatory response to SARS-CoV-2 infection. The CCC network (**Fig 6B**) showed abundant and active intercellular interactions, indicating dysregulated hyperinflammation in the COVID-19-infected lung tissue microenvironment.

We focused on communications between alveolar epithelial cells (AECs), macrophages, and monocytes, as the latter two are pivotal innate immune cells against SARS-CoV-2 infection (Merad & Martin, 2020), while AECs express a high level of the SARS-CoV-2 receptor ACE2 (Zhao *et al*, 2020), acting as a master communicator during viral infection (Miura, 2019). The edge bundling plot of LR interactions (**Fig 6C**) shows paracrine LR signaling from other cell types to AECs (left panel), macrophages (middle panel), and monocytes (right panel). Interestingly, relatively stronger activities of LR signaling were observed for each pair of the above three cell types. For example, FN1-SDC4 and TGM2-ITGB1 signaling from macrophages to AECs and C3-CD81 and GPC3-CD81 signaling from AECs to macrophages exhibited clearly stronger activities than other LR pairs. Moreover, we found that a number of ligand genes (e.g., FN1 and TGM2 in macrophages; C3 and GPC3 in AECs; and CD14, NID1, VCAN in monocytes) were also target genes in the multilayer networks of the three cell types (**Table S2**), and that almost all of these ligands as targets were positively correlated with their upstream LR signaling (**Fig 6D**). Collectively, these results indicate positive feedback loops between AECs, macrophages, and monocytes through paracrine LR signaling interactions (**Fig 6E**). The positive feedback of cytokine signaling may account for the sustained production and accumulation of inflammatory cytokines and dysregulated hyperinflammation in severe COVID-19 patients (Chen *et al*, 2021).

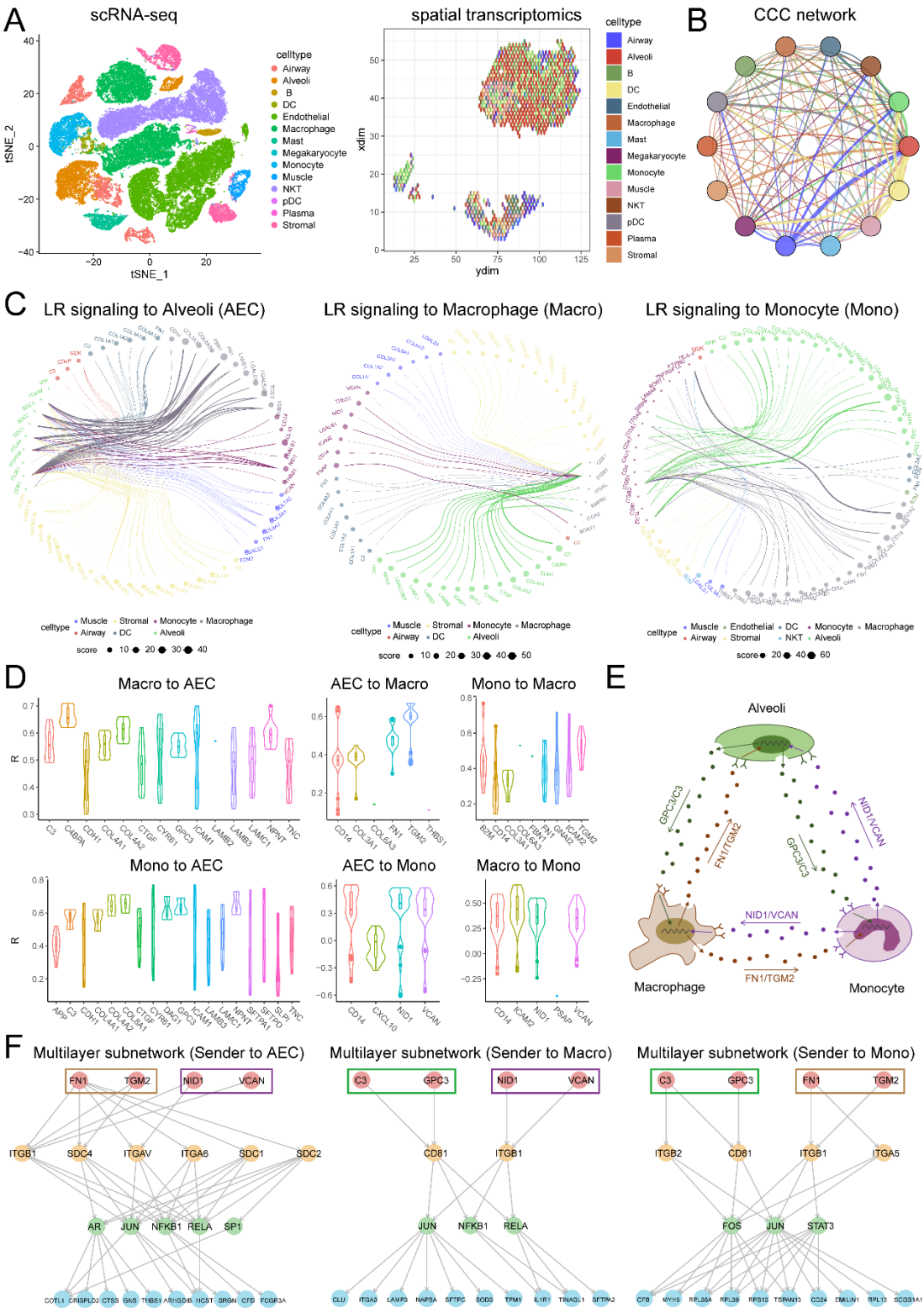

Fig 6. ***Application of stMLnet to a ST dataset of COVID-19***. *(**A**) The cell type annotation and deconvolution of the ST data of COVID-19 patient, with a set of scRNA-seq data as a reference. (**B**) The CCC network. (**C**) The edge bundling plot of intercellular LR signaling activity (top ranked) with alveolar epithelial cells (left panel), macrophages (middle panel), or monocytes (right panel) as receiver cells. The node size or edge width indicates the averaged strength of the LR signaling. (**D**) Correlations between expressions of ligand genes as intracellular targets and their upstream LR signaling activities. Most PCC*

*values (R) were positive except for a small fraction of monocytes. (**E**) Positive feedback circuits between AECs, macrophages, and monocytes. Representative ligands as paracrine cytokines are shown. (**F**) The multilayer signaling paths from the representative paracrine ligands to targets in AECs, macrophages, or monocytes inferred by stMLnet. Top-ranked target genes according to importance scores were prioritized for visualization.*

Furthermore, the multilayer subnetworks (**Fig 6E, Fig S6**) demonstrate the signaling paths from representative ligands to targets in AECs, macrophages, or monocytes. Several TFs, such as NFKB1, RELA, and JUN, were inferred to be involved in the intracellular signaling pathways underlying the above intercellular feedback circuits. These TFs are reportedly critical in regulating the gene expressions of inflammatory cytokines during SARS-CoV-2 infection, and they are targets of FDA-approved drugs (Santoso *et al*, 2021), indicating their therapeutical values for COVID-19 by disrupting the above feedback circuits.

In addition, we investigated the biological functions of the above intercellular feedback circuits by performing functional enrichment analysis for their intracellular target genes. The GO BP and KEGG pathway enrichment (**Fig S7**) demonstrated that processes or pathways related to COVID-19, immune response, cell adhesion, and the extracellular matrix (ECM) were significantly enriched for communications among AECs, macrophages, and monocytes. These results indicate the important roles of the abovementioned intercellular feedback loops in pulmonary injury and immune disorders in response to SARS-CoV-2 infection, and they are consistent with the results of previous studies (Peteranderl *et al*, 2016; Romero *et al*, 2015).

stMLnet deciphers tumor–macrophage interactions underlying immunotherapy resistance in gliomas

Owing to the limited availability of ST datasets, we can directly apply stMLnet to scRNA-seq data that are more widely available by using the “latent” spatial distance between cells as the input of stMLnet, based on the assumption of structural correspondence between distances in expression space and physical space (Nitzan *et al*, 2019).

CSF1R inhibitor (BLZ945) treatment is a macrophage-targeting immunotherapy for gliomas (Pyonteck *et al*, 2013). However, acquired resistance to CSF1R inhibition may emerge during the treatment, as observed in animal experiments (Quail *et al*, 2016). To investigate the microenvironment-mediated mechanism underlying resistance to CSF1R inhibition (a macrophage-targeting immunotherapy) in gliomas, we applied stMLnet to a set of scRNA-seq data (GSE131928) (Neftel *et al*, 2019) (**Fig 7A**) by using the expression-based Euclid distance as the proximity of the spatial distance of cells. The inferred CCC network (**Fig 7B**) demonstrates that abundant intercellular LR signaling from glioma cells to macrophages existed, indicating that glioma cells may substantially impact macrophages’ functions through intercellular interactions.

The multilayer networks (**Fig 7C**) further demonstrate the signaling paths downstream of IL13–IL4R and IL34-CSF1R in macrophages (left panel) or those downstream of IGF1-ITGAV in tumor cells (right panel). TFs STAT and NFAT were found to be involved in the downstream of IL4R or CSF1R signaling, which is consistent with the experimental studies (Quail *et al*, 2016). The waterfall plot of the multilayer signaling network (**Fig 7D**) shows regulatory paths from

upstream LR pairs (top ranked) to their downstream targets in macrophages (left panel) and malignant cells (right panel). GSEA analysis showed that highly expressed genes in macrophages were enriched in the activation and migration of macrophages (**Fig S8A**). The highly expressed genes in malignant cells were positively correlated with the gene sets related to the development and differentiation of neurons, neuronal stem cell population maintenance, and the VEGF signaling pathway (**Fig S8B**). GO enrichment analysis for downstream target genes in the multilayer networks revealed several important dysregulated pathways induced by glioma-activated CSF1R signaling (left panel) or IL4R signaling (right panel) in macrophages (**Fig S8C**) and dysregulated pathways induced by macrophages-activated ITGAV signaling in tumor cells (**Fig S8D**). The enriched pathways included several crucial pathways, such as the MAPK pathway and PI3K-AKT pathway, that are reportedly important in tumor initiation and progression. These results indicate the critical functional roles of IL4R and CSF1R signaling in macrophages, which can be exploited as potential targets for gliomas.

Among the abovementioned inferred intercellular LRs between glioma cells and macrophages, CSF1R signaling, IL4R signaling, and IGF1 signaling were validated to be involved in macrophage-glioma interactions and BLZ945 resistance (Quail *et al*, 2016) (**Fig 7E**, upper panel). stMLnet not only correctly predicted those known ligands or receptors, but it also revealed additional signaling pathways, while NicheNet and CytoTalk failed to predict all of the known interactions (**Fig 7E**, lower panel). In addition, to quantitatively assess the accuracy of stMLnet prediction regarding CSF1R-targets regulation, a set of RNA-seq data of macrophages isolated from mice (GSE69104) was analyzed. Differential expression status (true or false) of the target genes between the CSF1R-responder group (EP) and Veh group was used as the ground truth. AUCROC, AUCPR, Accuracy, PPV, Error rate, and MCC were computed for quantitative evaluation. The CSF1R-target predictions by NicheNet and CytoTalk were also evaluated for benchmarking. The result (**Fig 7F**) shows that stMLnet performed significantly better than NicheNet for all of the evaluation metrics, while CytoTalk could not successfully predict CSF1R from the data.

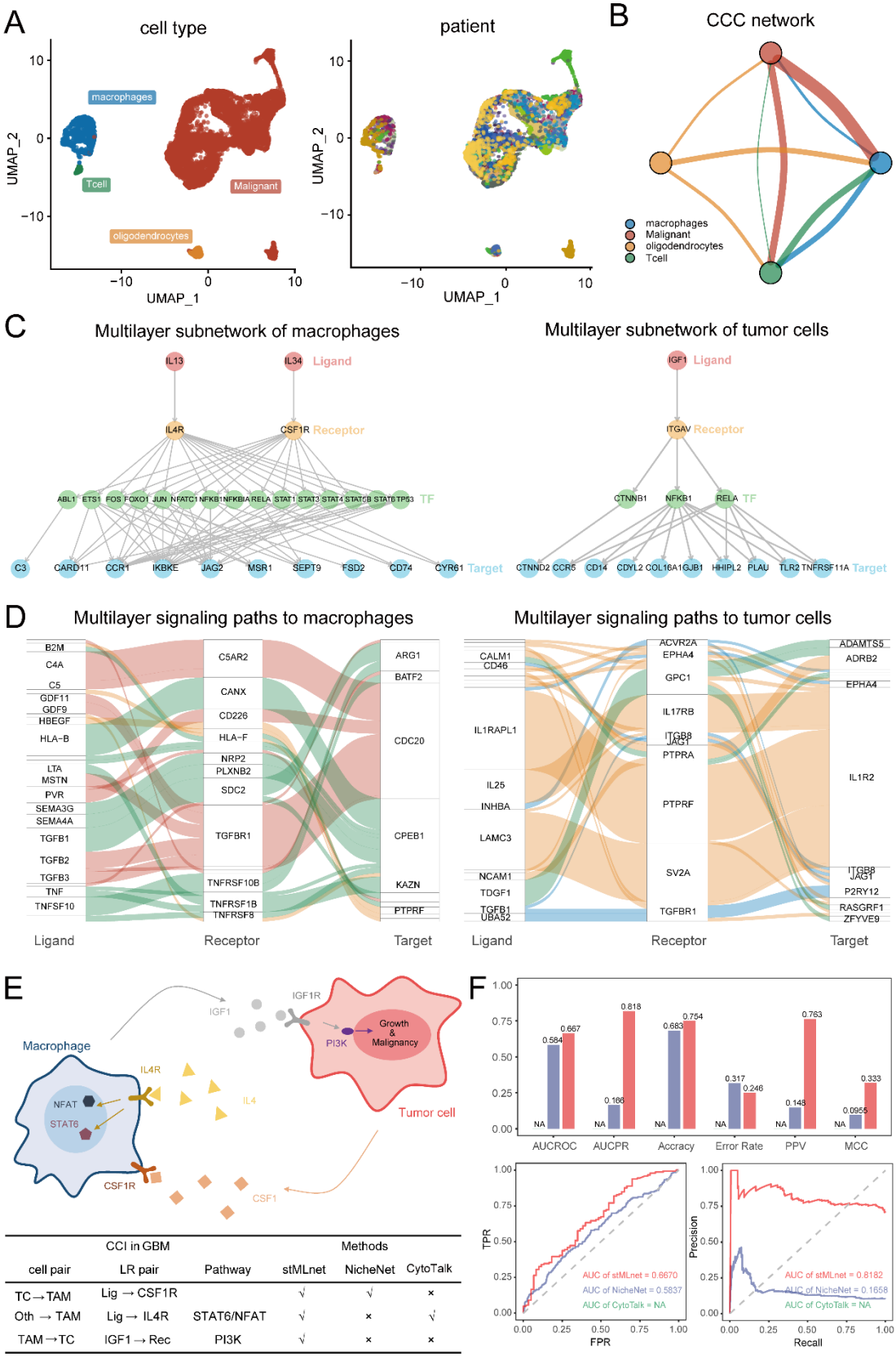

CCI in GBM			Methods		
cell pair	LR pair	Pathway	stMLnet	NicheNet	CytoTalk
TC→TAM	Lig → CSF1R		√	√	×
Oth → TAM	Lig → IL4R	STAT6/NFAT	√	×	√
TAM→TC	IGF1 → Rec	PI3K	√	×	×

Fig 7. *Application of stMLnet to single-cell RNA-seq data of gliomas*. *(**A**) UMAP visualization and cell type annotation. (**B**) The CCC network. (**C**) The multilayer signaling subnetwork downstream of IL13-IL4R signaling and IL34-CSF1R signaling in macrophages (left panel) or that downstream of IGF1-ITGAV*

*signaling in tumor cells (right panel). Only top-ranked target genes are shown for visualization purposes. (**D**) The multilayer signaling paths from upstream LR pairs (top-ranked) to their downstream targets in macrophages (left panel) or tumor cells (right panel). Different colors of paths represent cellular sources (sender cells) of the ligand signaling, and the width of the path represents the importance score for each LR~TG regulation. (**E**) The known interactions between macrophages and glioma cells that were validated and reported in the literature (upper panel) and the predictions of stMLnet, NicheNet, or CytoTalk (lower panel). (**F**) Evaluating stMLnet prediction regarding CSF1R-targets regulation in macrophages based on gene expression changes after CSF1R inhibitor treatment in responder mice. stMLnet outperformed NicheNet, and CytoTalk could not predict out CSF1R ('NA').*

Discussion

We have described stMLnet, a tool to decipher mechanisms underlying cellular communications and molecular regulations from ST data. It combines data integration, statistical inference, mechanistic modeling, and machine learning to construct a multilayer signaling network, infer LR signaling activity, and predict LR-target gene regulation. stMLnet leverages spatial information in the ST data to quantify intercellular signaling activity and, more importantly, connect extracellular signals to intracellular gene expression. stMLnet can be used to depict the microenvironmental regulation of gene expression by prioritizing upstream regulators for a given set of target genes or inferring downstream pathways and regulator networks for a given ligand or receptor.

One of the challenges in CCC inference is the lack of appropriate benchmarking, which impedes the methodological development and practical applications of such tools. As such, the predictions derived from different methods or tools sometimes differ from each other, and their prediction accuracies have not been well tested. In this study, we collected cell line perturbation datasets for quantitative benchmarking. Although *in vitro* data are not the perfect gold standard, to the best of our knowledge, cell line perturbation data have been the best choice for benchmarking ligand-target predictions until now, as differential responses of target genes to ligand or receptor perturbations characterize the potential regulations between them. Among the existing methods (Armingol *et al*, 2022a; Armingol *et al*, 2022b; Arnol *et al*, 2019; Baccin *et al*, 2020; Baruzzo *et al*, 2022; Browaeys *et al*, 2020; Cabello-Aguilar *et al*, 2020; Cang & Nie, 2020; Dries *et al*, 2021b; Efremova *et al*, 2020; Hou *et al*, 2020b; Jin *et al*, 2021; Noël *et al*, 2021; Pham *et al*, 2020; Tanevski *et al*, 2021; Wang *et al*, 2019a; Wang *et al*, 2019b; Yuan & Bar-Joseph, 2020; Zhang *et al*, 2021) (**Table S1**), we chose NicheNet, CytoTalk, and MISTy as competitors for benchmarking stMLnet, as they can output prediction scores of ligand-target regulations that can be compared to the ground truth (differential expression of targets in response to ligand/receptor perturbations). The results show that stMLnet outperformed the other methods on multiple datasets.

The advances of stMLnet that led to its superior performance are as follows. First, the L-R-TF-TG multilayer network modeling framework is adequate and effective in depicting intercellular communication-mediated gene expression. The multilayer network method evaluates the upstream activities using the downstream responses, which may reduce false-positive predictions. To fulfill this objective, we integrate carefully curated prior network database

information with context- and cell type-specific expression data to discover potential causal relationships between the upstream signaling and the downstream targets by employing the random walk algorithm and statistical inference method (e.g., Fisher's exact test). Second, the spatial information in the ST data is leveraged to mechanistically quantify LR signaling activities based on a mathematical diffusion model of microenvironmental ligands. This leads to a parameter-free reciprocal relationship between effective ligand signals receipted by the receiver cells and cell–cell physical distance, which, although simplified, avoids unfeasible estimation or calibration of ligand-specific parameters (e.g., diffusion rate and degradation rate). Third, we employ an explainable random forest regression model to measure the contribution of each ligand or receptor or LR pair in regulating target gene expression.

Admittedly, our study had some limitations. For example, our method makes several simplified assumptions. In our diffusion model, we approximate the ligand concentration around the sender cells with ligand gene expression by assuming a positive correlation between them. Similarly, regarding the LR signaling activity, we use receptor gene expression to substitute its protein level in the receiver cells. Additionally, the TF-target information comes from prior databases, which are not cell-type-specific. These drawbacks can be addressed by integrating ST data with emerging single-cell multi-omics data, such as single-cell proteomics data and single-cell ATAC sequencing data, thanks to the fast development of sequencing technology. In future studies, we will develop novel multiscale models that integrate multi-omics data across multiple layers to make better inferences of CCC and gene–gene regulations.

In summary, stMLnet, a modeling framework for deciphering intercellular signaling and intracellular regulations, provides an effective method to enrich the downstream analysis of spatial transcriptomics data for biological and clinical applications.

Methods

The proposed method stMLnet mainly encapsulates four components (**Fig 1**), i.e., constructing prior network databases based on multiple data sources, inferring multilayer signaling network based on gene expression data, calculating distance-dependent LR signaling activity, and quantifying regulatory relationships between upstream L/R and downstream target genes in the inferred multilayer network.

Collection and integration of prior network information

To infer inter- and intra-cellular signaling networks, we collected multiple data sources of molecular interactions as prior network information (**Text S1**). We processed and integrated them into prior knowledge databases of stMLnet at three scales of signaling transduction: LigRecDB (ligand-receptor prior database), TFTargetDB (TF-target gene prior database), and RecTFDB (receptor-TF prior database) (**Fig S1**) (**Table S3**).

LigRecDB

The ligand-receptor interaction information comes from connectomeDB2020 (Hou *et al*, 2020a), iTALK (Wang *et al*, 2019b), NicheNet (Browaeys *et al*, 2020) and CellChat (Jin *et al*, 2021). Most of the ligand-receptor pairs deposited in these databases are evidenced by the literature

reports or supported by multiple other databases. Ultimately, we curated a ligand-receptor database LigRecDB that consists of 3659 pairs of non-redundant LR interactions, including 920 ligands and 751 receptors.

TFTGDB

The interaction information between TF and target genes comes from TRRUST (Han *et al*, 2018), HTRIdb (Bovolenta *et al*, 2012), RegNetwork (Liu *et al*, 2015) and GTRD (Kolmykov *et al*, 2021). TRRUST and HTRIdb deposit a number of literature-supported TF-target genes interactions. RegNetwork integrates 25 previously existing databases including predicted/experimental transcriptional regulatory interactions. Ultimately, we collected 373501 pairs of TF-target gene interactions, with 525 TFs and 23021 targets, which compose the TFTargetDB database.

RecTFDB

To infer links from receptors to TFs, we used R package graphite (Sales *et al*, 2019) to extract information of intracellular molecular interactions or signaling pathways from 8 existing databases. Based on such information, we constructed directed weighted network and employed a random walk algorithm (László *et al*, 1996) to infer receptor-TF links (**Text S2**) and the hyper-parameters were calibrated using perturbation-expression data of 69 cell lines involving 27 ligands and 13 receptors (**Fig S2**). At last, 17450 pairs of non-redundant receptor-TF links were predicted out, comprising 751 receptors and 525 TFs, which compose the RecTFDB database.

The comparison of the prior databases of stMLnet with those of NicheNet (Browaeys *et al*, 2020) and Omnipath (Türei *et al*, 2016) is described in **Text S6**.

Inference of multilayer intercellular and intracellular signaling networks

The multilayer signaling network comprises of four layers of signaling molecules (i.e., ligand, receptor, TF and target genes) and three coherent sub-networks (i.e., LR signaling, receptor-TF pathways, and TF-target gene interactions). Based on our previous works (Cheng *et al*, 2021; Ni *et al*, 2022; Zhang *et al*, 2020), we used Fisher's exact test to qualitatively infer activated TFs from target gene expressions and then to infer activated LR pairs from the TF activity, by leveraging both the above prior network databases and the dataset-/cell type-specific gene expressions. In this way, only activated LR pairs and activated TFs were retained in the inferred multilayer network (see details in **Text S3**).

Modeling distance-dependent ligand-receptor signaling activity

To quantify signaling activities of LR pairs, we employed a mechanistic modeling approach by considering ligand diffusion in the microenvironment. Assume that the spatial coordinates of cell i and cell j are (x_i, y_i, z_i) and (x_j, y_j, z_j), respectively. The Euclid distance between cell i and cell j is $d_{ij} = \sqrt{(x_i - x_j)^2 + (y_i - y_j)^2 + (z_i - z_j)^2}$. Denote LR^k as the k-th pair of ligand-receptor, and L_i^k and R_j^k the corresponding ligand expression in the i-th cell and receptor expression in the j-th cell, respectively.

The ligand is a type of cytokine, which can diffuse in the microenvironment following release by the sender cells. The spatial-temporal distribution of the ligand concentration $u(x,y,z)$ during diffusion can be described by a partial differentia equation (PDE) as follows,

$$\frac{\partial u(x,y,z)}{\partial t} = D\Delta u(x,y,z), \quad (x,y,z) \in \boldsymbol{R}^3 \backslash B_1, \tag{1}$$

where Δ is the Laplace operator, defined as $\Delta u = \frac{\partial^2 u}{\partial x^2} + \frac{\partial^2 u}{\partial y^2} + \frac{\partial^2 u}{\partial z^2}$. D is the diffusion coefficient. B_1 represents unit ball indicating the sender cell. We assume that the diffusion of the ligand is relatively fast and the above equation quickly reaches to the steady-state. Therefore,

$$\Delta u(x,y,z) = 0, \quad (x,y,z) \in \boldsymbol{R}^3 \backslash B_1. \tag{2}$$

We further assume that the diffusion of the ligand across the local microenvironment is homogenous, and thereby the solution to the above equation is radially symmetric, i.e., $u(x,y,z) = u(r)$, where $r = \sqrt{x^2+y^2+z^2}$. Consequently, the above steady-state diffusion model could be simplified to an ordinary differential equation (ODE):

$$ru''(r) + 2u'(r) = 0. \tag{3}$$

Solving the above ODE, we get

$$u(r) = C_1 \frac{1}{r} + C_2, \tag{4}$$

where C_1 and C_2 are constants. Assume that the ligand concentration is u_1 along the boundary of B_1 and 0 far away. So we impose the boundary conditions $u(1) = u_1$, $u(\infty) = 0$. As such, $u(r) = \frac{1}{r}u_1$. We used the ligand expression in the sender cell (L_i^k) as a proximity of u_1. Therefore, the signaling strength of L_i^k received by the j-th cell is $\frac{1}{d_{ij}} L_i^k$.

Furthermore, based on the law of mass-action, the signaling strength of the k-th LR pair activated at the j-th cell could be defined as

$$LR_j^k = \sum_{i=1}^{n} \left(\frac{1}{d_{ij}} L_i^k R_j^k \right). \tag{5}$$

These equations quantitatively describe the influence of cell distance on ligand-receptor signaling intensity, so that the ligands from the sender cells with different distances react with the receptor of the receiver cell in different extent. As a result, the samples of LR signals (i.e., receiver cells) are consistent with those of the corresponding target genes, allowing mapping LR signal to the intracellular target gene expression.

Random forest regression for LR-target regulation

Assume m target genes (i.e., $G_1, G_2, \ldots, G_m$) in the inferred multilayer network and n_t pairs of LRs linked to each target gene G_t (i.e., $LR_1, LR_2, \ldots, LR_{n_t}$). To decipher quantitative regulation relationship between LR pairs and the target genes, we divided this task into m sub-problems by decoding the following functions:

$$G_t = f_t\left(LR_1, LR_2, \ldots, LR_{n_t}\right), \ t = 1, 2, \ \ldots, m. \tag{6}$$

Due to complex regulation relationship between LRs and the target gene, the above f_t is generally non-linear. We thus employed explainable tree-based regression to learn f_t. We constructed random forest regression model for each of the m target genes (**Fig 1E**). We used the signaling activities $LR_1, LR_2, \ldots, LR_{n_t}$ (calculated from Equation (5)) across the receiver cells as input to predict the expression of the target gene G_t. Based on the random forest model, we could calculate the importance score of the k_t-th feature (LR_{k_t}) contributing to the G_t expression, and thereby rank LR pairs. Moreover, we also refined the permutation importance score to account for the disassembled importance of L or R alone, which was referred to partial importance score (**Text S5**).

Data collection and processing

Breast cancer dataset

The spatial transcriptomics (ST) data of breast cancer was obtained from the 10x Genomics website. The preprocessing of the ST data, including quality control, normalization, and dimension reduction (tSNE analysis), was conducted using standard pipeline of Seurat. The cell type annotation information in a scRNA-seq dataset (GSE118389) (Karaayvaz *et al*, 2018) was mapped to each spot of the ST data ('FindTransferAnchors' and 'TransferData' in Seurat v3.2.3 (Stuart *et al*, 2019)). Furthermore, the cell type-specific gene expression for the dominant cell type in each spot was calculated using 'get_decomposed_data' function in RCTD v1.1.0 (Cable *et al*, 2021) with the aid of the cell type proportion matrix from Seurat output and the above scRNA-seq reference dataset. We also employed Giotto (Dries *et al*, 2021a) to get ICGs by using 'findICG' function and 'filterICG' function with default parameters, which were used as the input target gene set of interest for stMLnet. The ST data was imputed using Seurat 'runALRA' function to mitigate the sparsity of the expression matrix for the LR signaling quantification and random forest regression.

COVID-19 dataset

The ST data of COVID-19-infected human lung tissue was processed with the original code deposited at Mendeley: https://doi.org/10.17632/xjtv62ncwr.1. Following the original study (Gracia Villacampa *et al*, 2021), the NNMF method and the Pearson correlation were used to calculate spot-factor matrix and factor-celltype matrix to calculate cell type proportion for each spot in the ST data. More specifically, we firstly merged the similar subtypes according to the reference 10x scRNA-seq dataset (Travaglini *et al*, 2020) (**Table S4**) and then two truncation parameters (factor_cutoff = 0.5 and celltype_cutoff = 0.5) related to spot-factor matrix and factor-celltype matrix were utilized to avoid excessive dispersion of cell type proportion. The cell type proportion matrix was defined as the Hadamard product of the above two matrices. The cell type-specific gene expression for the first two dominant cell types in each spot was calculated using 'get_decomposed_data' function in RCTD v1.1.0 (Cable *et al*, 2021). The processed data is shown in **Fig S9**. Among the two samples, we selected sample 1 for further analysis and CCC inference. The cell type-specific DEGs in the ST data in each type of receiver cells (analyzed using 'FindMarkers' function in Seurat) were selected as the target genes of interest for input of stMLnet to infer multilayer signaling networks.

Glioma dataset

A set of scRNA-seq data of glioma (GSE131928) was used to analyze tumor-microenvironment interactions in gliomas. The standard pipeline of Seurat was performed for quality control, normalization, dimension reduction (tSNE analysis) and cell clustering. We used the marker genes provided in the original study (Neftel *et al*, 2019) for cell type annotation.

To select target genes of interest as input for stMLnet, we also collected a set of RNA-seq data of the isolated glioma cells or macrophages from three groups of mice with different responses to the CSF1R inhibitor treatment (Reb, rebound; EP, endpoint; Vel, vehicle) (GSE69104 (Quail *et al*, 2016)). After CPM standardization, low-expression genes with expression levels below 0.5 in more than 6 samples were filtered. We calculated differentially expressed genes (DEGs) in macrophages between different groups (Reb v.s. EP, EP v.s. Veh) using Wilcoxon rank sum test (|logfc|>2, p.adj<0.1). The DEGs between Reb and EP could be viewed as resistance-related genes, which were input to stMLnet as potential target genes in macrophages or tumor cells to infer their upstream regulators.

For other cell types (e.g., T cells and oligodendrocytes), we used highly expressed genes in these cell types, analyzed from the scRNA-seq data by using 'FindMarkers' function in Seurat (|logfc|>2, p.adj<0.05, pct>=0.1), as respective target genes of interest for stMLnet input.

In addition, the DEGs in macrophages between EP and Veh groups could be viewed as genes responsive to CSF1R inhibition and thus potentially regulated by CSF1R, which were used to test the prediction of stMLnet with respect to the CSF1R-regulated target genes.

Cell lines data

To calibrate parameters for prior information integration, we collected 129 datasets of cell line gene expression that were treated with ligands or perturbed by receptor knockout/mutation from the GEO database (**Table S5**), involving 23 tissues, 65 cell lines, 42 ligands and 18 receptors. We used limma (Ritchie *et al*, 2015) to select DEGs of each cell line (before vs. after perturbation) under criteria of |logfc|>1 and p.adj<0.05. Ultimately 70 datasets, each with more than 50 DEGs, were used for correction of prior databases in this study.

Simulation study

To evaluate the quantitative model involved in stMLnet, we benchmarked stMLnet with a set of synthetic data of spatial gene expressions. We consider 5 ligands, 2 receptors, 3 TFs and 4 target genes. The ground truth of the multilayer network is shown in **Fig S3A**.

We simulate 3 types of cells, including 2 types of sender cells (SC_1 and SC_2) and 1 type of receiver cells (RC). These cells are randomly located at a fraction of grids within a 2-dimensional lattice (100×100) that simulates a square domain of tissue slice ($\Omega \subset \boldsymbol{R}^2$). The ligand genes are expressed by the sender cells and the products are subject to diffusion. The receptor genes, TFs and TGs of the receiver cells do not diffuse across microenvironment.

The spatial-temporal changes of the extracellular ligands are modeled using the following reaction-diffusion equation

$$\frac{\partial [L_i]}{\partial t} = D_i \Delta [L_i] + \sum_k r_{ik} \chi_{SC_k}(x) - d_i [L_i] \quad (7)$$

where $[L_i] = [L_i](x,t)$ represents the concentration of the ligand L_i at location $x \in \Omega$ and time

t. D_i and d_i represents, respectively, the diffusion coefficient and degradation rate of the ligand L_i. r_{ik} is the release rate of the ligand L_i by sender cells SC_k $(k = 1 \text{ or } 2)$. $\chi_{SC_k}(x)$ is an indicator function of the sender cells, taking value 1 where there is a sender cell at location x, and 0 otherwise. Random initial value and the no-flux boundary condition are imposed to the above equation.

The level of each receptor is assumed steady through the simulation. The activation of each TF within the receiver cells is modulated by the upstream LR signaling, which is described as follows,

$$\frac{\partial[TF_l]}{\partial t} = \sum_j \alpha_{jl} \sum_i b_{ij}[L_i] \cdot [R_j] - \beta_l[TF_l] \tag{8}$$

where $[TF_l] = [TF_l](x,t)$ represents the activation level of the TF_l at location x and time t. b_{ij} equals to 1 or 0, representing binding or non-binding between ligand L_i and receptor R_j. α_{jl} is the activation coefficient of TF_l by R_j. β_l is the degradation rate of TF_l.

The expression of each target gene is regulated by TFs, which is described as follows,

$$\frac{\partial[TG_s]}{\partial t} = \sum_l \mu_{ls}\,[TF_l] - \gamma_s[TG_s] \tag{9}$$

where $[TG_s] = [TG_s](x,t)$ represents the expression level of the target gene TG_s at location x and time t. μ_{ls} is the regulatory coefficient of TG_s expression by TF_l. γ_s is the degradation rate of TG_s.

To get the steady-state values of spatial gene expression, we solve the following equations:

$$\begin{aligned} -D_i \Delta[L_i] &= \sum_k r_{ik}\chi_{SC_k}(x) - d_i[L_i] \\ \left.\frac{\partial[L_i]}{\partial \vec{n}}\right|_{\partial\Omega} &= 0 \end{aligned} \tag{10}$$

$$[TF_l](x) = \frac{1}{\beta_l}\sum_j \alpha_{jl} \sum_i b_{ij}[L_i] \cdot [R_j] \tag{11}$$

$$[TG_s](x) = \frac{1}{\gamma_s}\sum_l \mu_{ls}\,[TF_l] \tag{12}$$

Equations (10) were solved using finite difference method with five-point central difference scheme (**Text S7**). The values of some parameters (e.g., r_{ik}, α_{jl}, β_l, μ_{ls}, γ_s and $[R_j]$) in the above model were randomly sampled in each simulation. By simulating the above model with random parameter values 100 times, we got 100 sets of synthetic data each includes spatial expression values of 5 ligands, 2 receptors and 4 target genes and location coordinates of the SCs and RCs. **Fig 3C-H** illustrate a set of representative simulation data. Such spatial expression data was used as input of the random forest regression model in stMLnet (without using the prior information of the predefined multilayer network) to infer the regulation of TGs' expression by LR pairs. The predicted importance scores for LR-TG regulations were benchmarked with the ground truth.

Appendix

Appendix is available online and includes the following contents:

Text S1. Collection and integration of prior network information.

Data availability

The ST data of breast cancer was downloaded from the 10X Genomics website (https://support.10xgenomics.com/spatial-gene-expression/datasets/1.0.0/V1_Breast_Cancer_Block_A_Section_1). The ST data of COVID-19-infected lung tissue was downloaded from Mendeley (https://doi.org/10.17632/xjtv62ncwr.1). The scRNA-seq data of breast cancer, the scRNA-seq data of glioma, and the bulk RNA-seq data of macrophages were downloaded from the NCBI GEO database (GSE118389, GSE131928, and GSE69104, respectively). The scRNA-seq data of the lung was downloaded from Synapse (https://www.synapse.org/#!Synapse:syn21041850). The cell line gene expression datasets were downloaded from the NCBI GEO database, with the access numbers listed in **Table S5**. The simulation data is available from a public repository of Github (https://github.com/SunXQlab/stMLnet-simulation). The source code for the data analysis in the manuscript is available from Github (https://github.com/SunXQlab/stMLnet-AnalysisCode). The R package of stMLnet is publicly available from Github (https://github.com/SunXQlab/stMLnet). A web-based application of stMLnet is also developed and available at www.stmlnet.top/net.

Funding

XS was supported by grants from the National Key R&D Program of China (2021YFF1200903), the National Natural Science Foundation of China (11871070), the Guangdong Basic and

Applied Basic Research Foundation (2020B151502120). QN was partially supported by a National Science Foundation grant DMS1736272, a Simons Foundation grant (594598), and National Institute of Health grants U01AR073159 and U54CA217378.

Acknowledgements

We would like to acknowledge Xingjun Dong for assistance in web-server development.

Authors' contributions

J.C. performed research, analyzed data and wrote the draft; L.Y. assisted the software development; Q.N. participated in discussion and edited the paper; X.S. designed study, performed research, analyzed data and wrote the paper.

Conflict of interest

The authors declare that they have no conflict of interest.

References

Almet AA, Cang Z, Jin S, Nie Q (2021) The landscape of cell–cell communication through single-cell transcriptomics. *Current Opinion in Systems Biology* 26: 12-23

Armingol E, Baghdassarian HM, Martino C, Perez-Lopez A, Aamodt C, Knight R, Lewis NE (2022a) Context-aware deconvolution of cell-cell communication with Tensor-cell2cell. 2021.2009.2020.461129

Armingol E, Ghaddar A, Joshi CJ, Baghdassarian H, Shamie I, Chan J, Her H-L, O'Rourke EJ, Lewis NE (2022b) Inferring a spatial code of cell-cell interactions across a whole animal body. 2020.2011.2022.392217

Armingol E, Officer A, Harismendy O, Lewis NE (2021) Deciphering cell–cell interactions and communication from gene expression. *Nature Reviews Genetics* 22: 71-88

Arnol D, Schapiro D, Bodenmiller B, Saez-Rodriguez J, Stegle O (2019) Modeling Cell-Cell Interactions from Spatial Molecular Data with Spatial Variance Component Analysis. *Cell reports* 29: 202-211.e206

Baccin C, Al-Sabah J, Velten L, Helbling PM, Grünschläger F, Hernández-Malmierca P, Nombela-Arrieta C, Steinmetz LM, Trumpp A, Haas S (2020) Combined single-cell and spatial transcriptomics reveal the molecular, cellular and spatial bone marrow niche organization. *Nature cell biology* 22: 38-48

Baruzzo G, Cesaro G, Di Camillo B (2022) Identify, quantify and characterize cellular communication from single cell RNA sequencing data with scSeqComm. *Bioinformatics (Oxford, England)*: Identify, quantify and characterize cellular communication from single cell RNA sequencing data with scSeqComm

Boisset J-C, Vivié J, Grün D, Muraro MJ, Lyubimova A, van Oudenaarden A (2018) Mapping the physical network of cellular interactions. *Nature Methods* 15: 547-553

Boulanger CA, Mack DL, Booth BW, Smith GH (2007) Interaction with the mammary microenvironment redirects spermatogenic cell fate in vivo. *Proceedings of the National Academy of Sciences of the United States of America* 104: 3871-3876

Bovolenta LA, Acencio ML, Lemke N (2012) HTRIdb: an open-access database for experimentally verified human transcriptional regulation interactions. *BMC Genomics* 13: 405

Browaeys R, Saelens W, Saeys Y (2020) NicheNet: modeling intercellular communication by linking ligands to target genes. *Nat Methods* 17: 159-162

Cabello-Aguilar S, Alame M, Kon-Sun-Tack F, Fau C, Lacroix M, Colinge J (2020) SingleCellSignalR: inference of intercellular networks from single-cell transcriptomics. *Nucleic acids research* 48: e55

Cable DM, Murray E, Zou LS, Goeva A, Macosko EZ, Chen F, Irizarry RA (2021) Robust decomposition of cell type mixtures in spatial transcriptomics. *Nature Biotechnology*

Cang Z, Nie Q (2020) Inferring spatial and signaling relationships between cells from single cell transcriptomic data. *Nature communications* 11: 2084

Chen H, Liu W, Wang Y, Liu D, Zhao L, Yu J (2021) SARS-CoV-2 activates lung epithelial cell proinflammatory signaling and leads to immune dysregulation in COVID-19 patients. *EBioMedicine* 70: 103500

Cheng J, Zhang J, Wu Z, Sun X (2020) Inferring microenvironmental regulation of gene expression from single-cell RNA sequencing data using scMLnet with an application to COVID-19. *Brief Bioinform*: bbaa327

Cheng J, Zhang J, Wu Z, Sun X (2021) Inferring microenvironmental regulation of gene expression from single-cell RNA sequencing data using scMLnet with an application to COVID-19. *Briefings in bioinformatics* 22: 988-1005

Dries R, Zhu Q, Dong R, Eng C-HL, Li H, Liu K, Fu Y, Zhao T, Sarkar A, Bao F *et al* (2021a) Giotto: a toolbox for integrative analysis and visualization of spatial expression data. *Genome Biology* 22: 78

Dries R, Zhu Q, Dong R, Eng CL, Li H, Liu K, Fu Y, Zhao T, Sarkar A, Bao F *et al* (2021b) Giotto: a toolbox for integrative analysis and visualization of spatial expression data. *Genome biology* 22: 78

Efremova M, Vento-Tormo M, Teichmann SA, Vento-Tormo R (2020) CellPhoneDB: inferring cell-cell communication from combined expression of multi-subunit ligand-receptor complexes. *Nature protocols* 15: 1484-1506

Gracia Villacampa E, Larsson L, Mirzazadeh R, Kvastad L, Andersson A, Mollbrink A, Kokaraki G, Monteil V, Schultz N, Appelberg KS *et al* (2021) Genome-wide spatial expression profiling in formalin-fixed tissues. *Cell Genomics* 1: 100065

Han H, Cho JW, Lee S, Yun A, Kim H, Bae D, Yang S, Kim CY, Lee M, Kim E *et al* (2018) TRRUST v2: an expanded reference database of human and mouse transcriptional regulatory interactions. *Nucleic Acids Res* 46: D380-D386

Heasley LE (2001) Autocrine and paracrine signaling through neuropeptide receptors in human cancer. *Oncogene* 20: 1563-1569

Hou R, Denisenko E, Ong HT, Ramilowski JA, Forrest ARR (2020a) Predicting cell-to-cell communication networks using NATMI. *Nature Communications* 11: 5011-5011

Hou R, Denisenko E, Ong HT, Ramilowski JA, Forrest ARR (2020b) Predicting cell-to-cell communication networks using NATMI. *Nature communications* 11: 5011

Jin S, Guerrero-Juarez CF, Zhang L, Chang I, Ramos R, Kuan CH, Myung P, Plikus MV, Nie Q (2021) Inference and analysis of cell-cell communication using CellChat. *Nature communications* 12: 1088

Karaayvaz M, Cristea S, Gillespie SM, Patel AP, Mylvaganam R, Luo CC, Specht MC, Bernstein BE, Michor F, Ellisen LW (2018) Unravelling subclonal heterogeneity and aggressive disease states in TNBC through single-cell RNA-seq. *Nature Communications* 9: 3588

Kolmykov S, Yevshin I, Kulyashov M, Sharipov R, Kondrakhin Y, Makeev VJ, Kulakovskiy IV, Kel A,

Kolpakov F (2021) GTRD: an integrated view of transcription regulation. *Nucleic Acids Research* 49: D104-D111

Krauss G (2014) Basics of Cell Signaling. In: *Biochemistry of Signal Transduction and Regulation*, Krauss G. (ed.) pp. 1-26. Wiley-VCH Verlag GmbH & Co. KGaA: Weinheim, Germany

László L, Lov L, Erdos O (1996) *Random Walks on Graphs: A Survey*

Liu ZP, Wu C, Miao H, Wu H (2015) RegNetwork: an integrated database of transcriptional and post-transcriptional regulatory networks in human and mouse. *Database (Oxford)* 2015

Longo SK, Guo MG, Ji AL, Khavari PA (2021) Integrating single-cell and spatial transcriptomics to elucidate intercellular tissue dynamics. *Nature Reviews Genetics* 22: 627-644

Merad M, Martin JC (2020) Pathological inflammation in patients with COVID-19: a key role for monocytes and macrophages. *Nature reviews Immunology* 20: 355-362

Miura TA (2019) Respiratory Epithelial Cells as Master Communicators during Viral Infections. *Current Clinical Microbiology Reports* 6: 10-17

Neftel C, Laffy J, Filbin MG, Hara T, Shore ME, Rahme GJ, Richman AR, Silverbush D, Shaw ML, Hebert CM *et al* (2019) An Integrative Model of Cellular States, Plasticity, and Genetics for Glioblastoma. *Cell* 178: 835-849.e821

Ni X, Wu W, Sun X, Ma J, Yu Z, He X, Cheng J, Xu P, Liu H, Shang T *et al* (2022) Interrogating glioma-M2 macrophage interactions identifies Gal-9/Tim-3 as a viable target against PTEN-null glioblastoma. *Science Advances* 8: eabl5165

Nitzan M, Karaiskos N, Friedman N, Rajewsky N (2019) Gene expression cartography. *Nature* 576: 132-137

Noël F, Massenet-Regad L, Carmi-Levy I, Cappuccio A, Grandclaudon M, Trichot C, Kieffer Y, Mechta-Grigoriou F, Soumelis V (2021) Dissection of intercellular communication using the transcriptome-based framework ICELLNET. *Nature communications* 12: 1089

Parsons JT, Horwitz AR, Schwartz MA (2010) Cell adhesion: integrating cytoskeletal dynamics and cellular tension. *Nat Rev Mol Cell Biol* 11: 633-643

Peteranderl C, Morales-Nebreda L, Selvakumar B, Lecuona E, Vadász I, Morty RE, Schmoldt C, Bespalowa J, Wolff T, Pleschka S *et al* (2016) Macrophage-epithelial paracrine crosstalk inhibits lung edema clearance during influenza infection. *The Journal of clinical investigation* 126: 1566-1580

Pham D, Tan X, Xu J, Grice LF, Lam PY, Raghubar A, Vukovic J, Ruitenberg MJ, Nguyen Q (2020) stLearn: integrating spatial location, tissue morphology and gene expression to find cell types, cell-cell interactions and spatial trajectories within undissociated tissues. 2020.2005.2031.125658

Pires-daSilva A, Sommer RJ (2003) The evolution of signalling pathways in animal development. *Nature reviews Genetics* 4: 39-49

Pyonteck SM, Akkari L, Schuhmacher AJ, Bowman RL, Sevenich L, Quail DF, Olson OC, Quick ML, Huse JT, Teijeiro V *et al* (2013) CSF-1R inhibition alters macrophage polarization and blocks glioma progression. *Nature medicine* 19: 1264-1272

Quail DF, Bowman RL, Akkari L, Quick ML, Schuhmacher AJ, Huse JT, Holland EC, Sutton JC, Joyce JA (2016) The tumor microenvironment underlies acquired resistance to CSF-1R inhibition in gliomas. *Science (New York, NY)* 352: aad3018

Ritchie ME, Phipson B, Wu D, Hu Y, Law CW, Shi W, Smyth GK (2015) limma powers differential expression analyses for RNA-sequencing and microarray studies. *Nucleic Acids Research* 43: e47-e47

Romero F, Shah D, Duong M, Penn RB, Fessler MB, Madenspacher J, Stafstrom W, Kavuru M, Lu B, Kallen CB *et al* (2015) A pneumocyte-macrophage paracrine lipid axis drives the lung toward fibrosis. *American journal of respiratory cell and molecular biology* 53: 74-86

Sales G, Calura E, Romualdi C (2019) metaGraphite–a new layer of pathway annotation to get metabolite networks. *Bioinformatics* 35: 1258-1260

Santoso CS, Li Z, Rottenberg JT, Liu X, Shen VX, Fuxman Bass JI (2021) Therapeutic Targeting of Transcription Factors to Control the Cytokine Release Syndrome in COVID-19. 12

Scadden DT (2006) The stem-cell niche as an entity of action. *Nature* 441: 1075-1079

Stuart T, Butler A, Hoffman P, Hafemeister C, Papalexi E, Mauck WM, Hao Y, Stoeckius M, Smibert P, Satija R (2019) Comprehensive Integration of Single-Cell Data. *Cell* 177: 1888-1902.e1821

Tanevski J, Flores ROR, Gabor A, Schapiro D, Saez-Rodriguez J (2021) Explainable multi-view framework for dissecting intercellular signaling from highly multiplexed spatial data. *bioRxiv*: 2020.2005.2008.084145

Travaglini KJ, Nabhan AN, Penland L, Sinha R, Gillich A, Sit RV, Chang S, Conley SD, Mori Y, Seita J *et al* (2020) A molecular cell atlas of the human lung from single-cell RNA sequencing. *Nature* 587: 619-625

Türei D, Korcsmáros T, Saez-Rodriguez J (2016) OmniPath: guidelines and gateway for literature-curated signaling pathway resources. *Nat Methods* 13: 966-967

Walker BL, Cang Z, Ren H, Bourgain-Chang E, Nie Q (2022) Deciphering tissue structure and function using spatial transcriptomics. *Communications Biology* 5: 220

Wang S, Karikomi M, MacLean AL, Nie Q (2019a) Cell lineage and communication network inference via optimization for single-cell transcriptomics. *Nucleic acids research* 47: e66

Wang Y, Wang R, Zhang S, Song S, Jiang C, Han G, Wang M, Ajani J, Futreal A, Wang L (2019b) iTALK: an R Package to Characterize and Illustrate Intercellular Communication. *bioRxiv*: 507871

Yuan Y, Bar-Joseph Z (2020) GCNG: graph convolutional networks for inferring gene interaction from spatial transcriptomics data. *Genome biology* 21: 300

Zhang J, Guan M, Wang Q, Zhang J, Zhou T, Sun X (2020) Single-cell transcriptome-based multilayer network biomarker for predicting prognosis and therapeutic response of gliomas. *Briefings in bioinformatics* 21: 1080-1097

Zhang Y, Liu T, Hu X, Wang M, Wang J, Zou B, Tan P, Cui T, Dou Y, Ning L *et al* (2021) CellCall: integrating paired ligand-receptor and transcription factor activities for cell-cell communication. *Nucleic acids research* 49: 8520-8534

Zhao Y, Zhao Z, Wang Y, Zhou Y, Ma Y, Zuo W (2020) Single-Cell RNA Expression Profiling of ACE2, the Receptor of SARS-CoV-2. *American journal of respiratory and critical care medicine* 202: 756-759

Datasets -Spatial Gene Expression -Official 10x Genomics Support. *https://support10xgenomicsco m/spatial-gene-expression/datasets/100/V1_Breast_Cancer_Block_A_Section_1*